Pharmaceutical Research, Vol. 26, No. 4, April 2009 (© 2008)
DOI: 10.1007/s11095-008-9784-z

Research Paper

Solubility of Small-Molecule Crystals in Polymers: D-Mannitol in PVP, Indomethacin in PVP/VA, and Nifedipine in PVP/VA

Jing Tao,[1] Ye Sun,[1] Geoff G. Z. Zhang,[2,3] and Lian Yu[1,3]

Received July 15, 2008; accepted November 4, 2008; published online December 4, 2008

Objective. Amorphous pharmaceuticals, a viable approach to enhancing bioavailability, must be stable against crystallization. An amorphous drug can be stabilized by dispersing it in a polymer matrix. To implement this approach, it is desirable to know the drug's solubility in the chosen polymer, which defines the maximal drug loading without risk of crystallization. Measuring the solubility of a crystalline drug in a polymer is difficult because the high viscosity of polymers makes achieving solubility equilibrium difficult.

Method. Differential Scanning Calorimetry (DSC) was used to detect dissolution endpoints of solute/polymer mixtures prepared by cryomilling. This method was validated against other solubility-indicating methods.

Results. The solubilities of several small-molecule crystals in polymers were measured for the first time near the glass transition temperature, including D-mannitol (β polymorph) in PVP, indomethacin (γ polymorph) in PVP/VA, and nifedipine (α polymorph) in PVP/VA.

Conclusion. A DSC method was developed for measuring the solubility of crystalline drugs in polymers. Cryomilling the components prior to DSC analysis improved the uniformity of the mixtures and facilitated the determination of dissolution endpoints. This method has the potential of providing useful data for designing physically stable formulations of amorphous drugs.

KEY WORDS: amorphous pharmaceuticals; glass transition; polymer dispersion; PVP; PVP/VA; solubility.

INTRODUCTION

Pharmaceutical scientists increasingly face the challenge of delivering poorly water soluble drugs. A viable approach to enhancing the bioavailability of poorly soluble drugs is to use amorphous solids in place of crystals in pharmaceutical formulations. This approach takes advantage of the higher solubility of amorphous solids than their crystalline counterparts. To implement this approach, however, adequate understanding is needed of the stability of amorphous drugs against crystallization, because crystallization negates their advantages.

A physical property of special importance is the solubility of crystalline drugs in polymeric matrices. This property is important for selecting appropriate polymers for formulation; it defines the upper limit of drug loading without the risk of crystallization. Despite its importance, there has been no standard technique for measuring the drug/polymer solubility. The difficulty exists because the high viscosity of polymers makes achieving solubility equilibrium difficult. Vasanthavada *et al.* used moisture to induce the crystallization of trehalose from its mixture with dextran or PVP and compared the eventual glass transition temperature T_g of the system and the T_g of the pure polymer to calculate trehalose's solubility in the polymer (1,2). The method measures the drug/polymer solubility *in the presence of water*, not in the dry state. Marsac *et al.* developed a model to predict drug/polymer solubility based on the Flory–Huggins theory of liquids (3,4). The model was calibrated on the solubilities of drugs in 1-methyl-2-pyrrolidone (NMP), a small-molecule solvent related to PVP, but has not been tested with experimentally measured drug/polymer solubility.

Another difficulty encountered in studying drug/polymer solubility is the fact that pharmaceutically important drug/polymer dispersions tend to be glasses or liquids that are kinetically frozen without crystallization. Despite their low molecular mobility, glasses relax over time toward the equilibrium liquid state (the state that the system would reach if it were cooled infinitely slowly). Being an equilibrium property, the drug/polymer solubility is properly defined only if the liquid in equilibrium with the crystalline phase is at equilibrium itself (not a glass). If a glass relaxes slowly, however, an apparent solubility could be defined. This apparent solubility would not be unique, but decrease with glass relaxation until the system reaches equilibrium. The model proposed by Marsac *et al.*, and models based on equilibrium thermodynamics in general, predict the solubility for the fully relaxed, equilibrium liquid. In practice, structural relaxation of a glass

[1] School of Pharmacy and Department of Chemistry, University of Wisconsin, Madison, 777 Highland Avenue, Madison, Wisconsin 53705, USA.
[2] Solid State Sciences, Global Pharmaceutical R & D, Abbott Laboratories, North Chicago, Illinois 60064, USA.
[3] To whom correspondence should be addressed. (e-mail: Geoff.GZ.Zhang@abbott.com, lyu@pharmacy.wisc.edu)

may be so slow that the time to reach equilibrium may far exceed the typical shelf life of pharmaceuticals (years). The relevant solubility therefore need not be the solubility in the equilibrium liquid, but the solubility in the glassy matrix that can be maintained during the shelf life of the product.

The goal of this work was to measure the drug/polymer solubility near the glass transition temperature. Because of the low molecular mobility in the glassy state, reaching solubility equilibrium below T_g would be extremely slow. We studied whether DSC, a convenient technique available in many laboratories, can be used to measure the solubility of small-molecule crystals in polymers. DSC has been used to measure the solubility of small-molecule crystals in small-molecule solvents (5–7). The method involves heating a crystal/solvent slurry of known composition (x) to slowly dissolve the crystals in the solvent. If phase equilibrium is maintained during heating, the solubility of the crystal in the solvent is x at the final temperature of crystal dissolution, T_{end}. We applied the same method to drug/polymer systems. To aid the attainment of phase equilibrium, we used slow heating rates and extrapolated T_{end} to zero heating rate. Moreover, we used cryomilling to mix the components before DSC analysis to improve the uniformity of mixing and facilitate the determination of dissolution endpoints. This method was applied first to D-mannitol in PVP, and the result was validated against two other solubility-indicating methods. The method was further tested against independently measured solubility of nifedipine (NIF) in 1-methyl-2-pyrrolidone (NMP) (3). We then applied the method to indomethacin (IMC) in PVP/VA and NIF in PVP/VA (Scheme 1). IMC (8–11) and NIF (12–15) are two model systems for studying the stability of amorphous drugs; they are both poorly water-soluble and have similar molecular weight, T_g (42°C), and T_m. NIF crystallizes faster than IMC. PVP and PVP/VA are two pharmaceutical polymers of different hydrophilicity that have been used as matrices for dispersing amorphous drugs (16–18). We have determined for the first time the solubilities of small-molecule crystals in polymers near T_g and by extrapolation, obtained the solubilities at T_g. Our method has the potential of providing useful data for designing physically stable formulations of amorphous drugs.

EXPERIMENTAL SECTION

D-Mannitol (99+%, β polymorph), nifedipine (NIF, α polymorph), a calcium channel blocker, and indomethacin (IMC, γ polymorph), a nonsteroidal anti-inflammatory agent, were obtained from Sigma-Aldrich. Polyvinyl pyrrolidone (PVP, K=15) was obtained from GAF Chemicals. PVP/VA (Kollidone VA64, M_w=45,000–70,000) was supplied by BASF. It was a 60:40 vinyl pyrrolidone–vinyl acetate copolymer (T_g= 101°C). It was found less hygroscopic than PVP K15.

A cryogenic impact mill (SPEX CertiPrep model 6750) was used to prepare solute/polymer mixtures of different compositions. Liquid nitrogen was used as coolant. In a typical procedure, 0.5–1 g of solute/polymer powder was milled at 10 Hz. Each cycle of milling was 2 min, followed by a 2 min cool-down. The cycle was repeated to achieve a desired milling time (2–60 min). Ball milling was performed in a mixer mill (Retsch, Inc., model MM 200). One gram of solute/polymer powder mixture was milled at 30 Hz. Each cycle of milling was 5 min, followed by a 10 min interruption. The cycle was repeated to achieve a total milling time of 30 min). Hand milling was performed by grinding 2–5 g of a solute/polymer mixture with mortar and pestle. The milled materials were analyzed by X-ray powder diffraction to assess the change of polymorphic form and loss of crystallinity. For all materials used for solubility measurement, the crystals that remained after milling were of the original polymorphs (β for D-mannitol, α for nifedipine, and γ for indomethacin).

Differential scanning calorimetry (DSC) was conducted in hermetic aluminum pans using a TA Instruments DSC Q2000. 5–10 mg of the sample was packed into the pans. A pin hole was made in the lid to allow the escape of moisture. Before scanning to detect the dissolution endpoint, the sample was pre-heated in the DSC pan to 100°C or 105°C

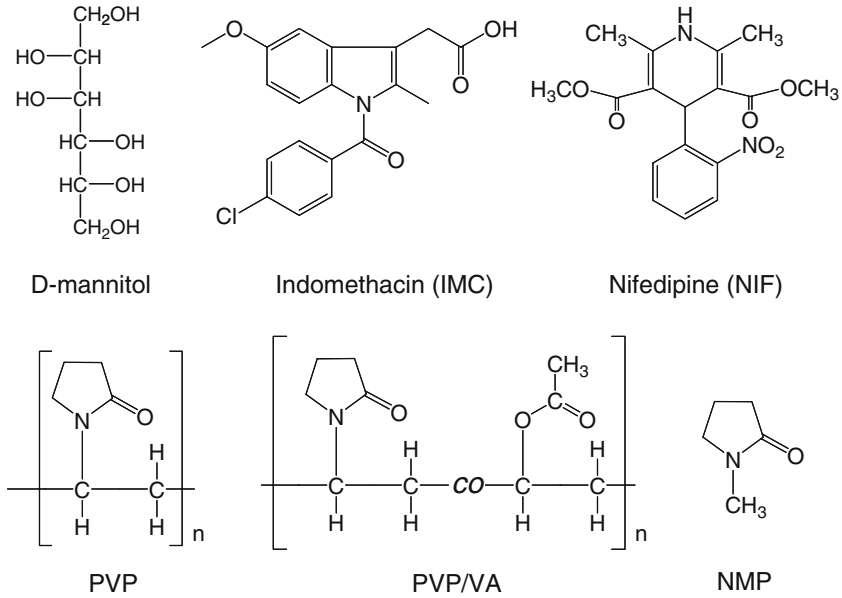

Scheme 1. Structures of D-mannitol, indomethacin, nifedipine, PVP, PVP/VA, and 1-methyl-2-pyrrolidone (NMP).

to dry off the residual moisture. It was then cooled and reheated at a rate from 0.1°C/min to 5°C/min to above the dissolution endpoint. The dissolution endpoint T_{end} was calculated from the heat flow signal as the intersection of the falling edge of the dissolution endotherm and the post-dissolution baseline (Fig. 1a). After the T_{end} measurement, the sample was cooled again and heated at 10°C/min to record the glass transition temperature T_g. No significant difference was observed between the T_g measured after a fast or a slow previous heating, which suggests that the sample did not degrade significantly during DSC scans, even at the slowest heating rate. Modulated DSC was used to measure the glass transition of the amorphous phase at a heating rate of 2°C/min with the temperature modulating at ±0.5°C every 60 s.

X-ray diffraction was performed with a Bruker D8 Advance diffractometer (Cu Kα radiation, voltage 40 kV, and current 40 mA). The sample was ground with mortar and pestle, placed on a zero-background silicon (510) sample holder, and scanned from 2° to 50° (2θ) at a speed of 1°/min and a step size of 0.02°. Raman microscopy was performed with a Renishaw System 1000 Micro-Raman spectrometer equipped with a HeNe laser and peltier-cooled CCD detector.

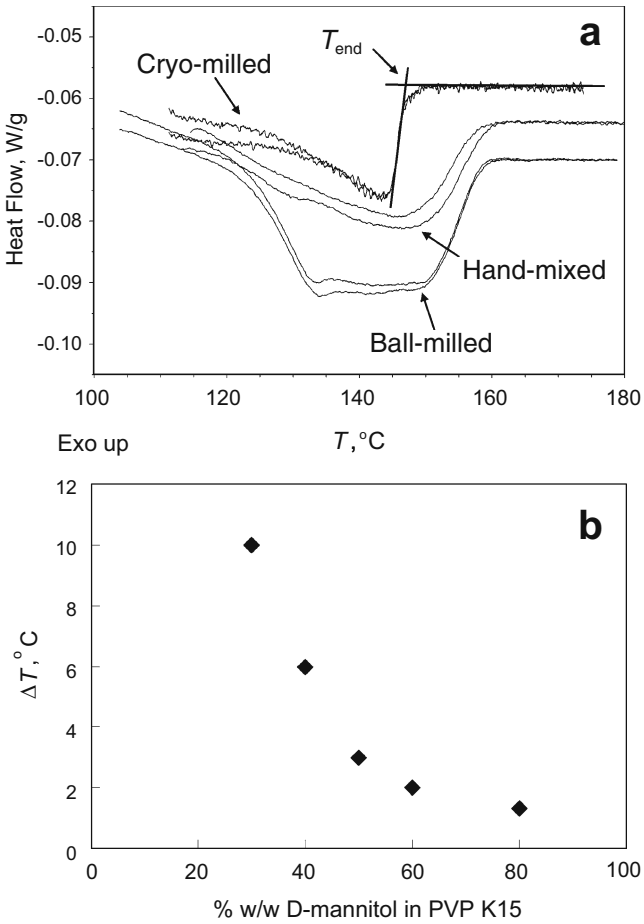

Fig. 1. a Dissolution endotherms of 30% *w*/*w* D-mannitol (β-polymorph) in PVP K15 prepared by cryomilling (16 min), hand mixing (20 min), and ball milling (30 min). Heating rate was 0.5°C/min. **b** Difference in dissolution endpoints between hand-mixed (20 min) and cryomilled (16–20 min) samples. The difference increased with increasing polymer concentration.

For aging experiments performed to verify solubilities determined by the DSC dissolution-endpoint method, samples in open DSC pans were heated on a microscope hot-stage (Linkam THMS 600) to T_m+20°C. Vacuum was applied during heating to remove air bubbles trapped in the viscous melt. The pans were then quenched to room temperature, sealed immediately, and aged in ovens of known temperatures.

RESULTS AND DISCUSSION

Mixing by Cryomilling Helps Determine Dissolution Endpoint

Because dissolution of a crystalline substance in a polymer matrix requires the transport of materials in space, how well the components are mixed before dissolution affects how accurately the endpoint of dissolution is detected by DSC. If the components are poorly mixed and contain large particles, dissolution requires material transport over long distances. This may not be a significant problem if the viscosity of the solution is low, but is a problem if the viscosity of the solution is so high that the mixing of components becomes too slow at the timescale of DSC measurement. When a poorly mixed sample is analyzed by DSC, the endpoint of dissolution will appear higher than the equilibrium solubility temperature. We tested three ways of mixing the components: hand mixing, ball milling, and cryomilling. Fig. 1a shows typical results observed with D-mannitol (β polymorph). XRD analysis showed that the crystals that remained after cryomilling were of the original polymorph. Because β D-mannitol is the most stable of its three known polymorphs monotropically, no polymorphic conversion could occur during the DSC analysis. As Fig. 1a illustrates, that the cryomilled sample generally had lower dissolution endpoints T_{end} than the corresponding ball-milled and hand-mixed samples. The smaller heat of dissolution of the cryomilled sample in Fig. 1a suggests that cryomilling reduced the crystallinity of D-mannitol or even partially dissolved the solute.

Fig. 1b shows how cryomilling facilitated the dissolution of D-mannitol in PVP K15 at various concentrations. ΔT is the difference in T_{end} between hand-mixed and cryomilled samples, both heated at 0.5°C/min in DSC. The benefit of cryomilling was greater for samples of lower solute concentrations: ΔT was about 2°C at high solute concentrations, but increased up to 10°C with decreasing solute concentration. This difference is caused by the increase of the system's viscosity with decreasing solute concentration (increasing polymer concentration). Overheating due to poor mixing is expected to be greater when the system's viscosity is higher and is apparently suppressed more effectively by cryomilling.

The optimal time of cryomilling was determined by increasing the milling time to the point of diminishing return (no further decrease of T_{end}). We tested milling times from a few minutes to 1 h, and found that the optimal milling time was approximately 16 min for all but the lowest D-mannitol concentration mixture (20% *w*/*w*), which was milled for 60 min. Similar effect was observed for IMC or NIF in PVP/VA (see later). Adequate milling was more important at lower D-mannitol concentrations. For example, at 30% *w*/*w* D-mannitol, the reduction of T_{end} by changing the milling time from 2 to 32 min was 10°C, with milling longer than

16 min offering little further lowering of T_{end}. In comparison, at higher D-mannitol concentrations, shorter milling times would suffice.

Fig. 2 shows the dissolution endpoints of cryomilled D-mannitol/PVP mixtures measured at different heating rates. Fig. 2a shows one set of raw DSC data collected for the 40% *w/w* D-mannitol mixture; Fig. 2b shows the T_{end} *vs.* heating rate plots for mixtures of different concentrations. Fig. 2b shows that for the cryomilled materials, T_{end} depends weakly on heating rate. In contrast, the hand-mixed materials showed much stronger dependence of T_{end} on heating rate. These results suggest that the dissolution process in the cryomilled materials was not limited by diffusive mixing; if it did, changing the heating rate would substantially change T_{end}. The T_{end} reported in this work refers to its extrapolated value at zero heating rate. With a weaker dependence of T_{end} on heating rate for cryomilled samples, this extrapolation can be made with greater confidence.

The effects of cryomilling likely include mixing the components, reducing the particle size, making the solute partially amorphous, and even partially dissolving the solute. With better mixing and smaller particles, the components need not diffuse very far to achieve a homogeneous solution (dissolution endpoint). We speculate that cryomilling differs from hand- and ball-milling because at cryogenic temperatures, particles undergo brittle fracture rather than plastic deformation, making particle size reduction and component mixing more efficient. This in turn may facilitate the detection of dissolution endpoint without substantial overheating.

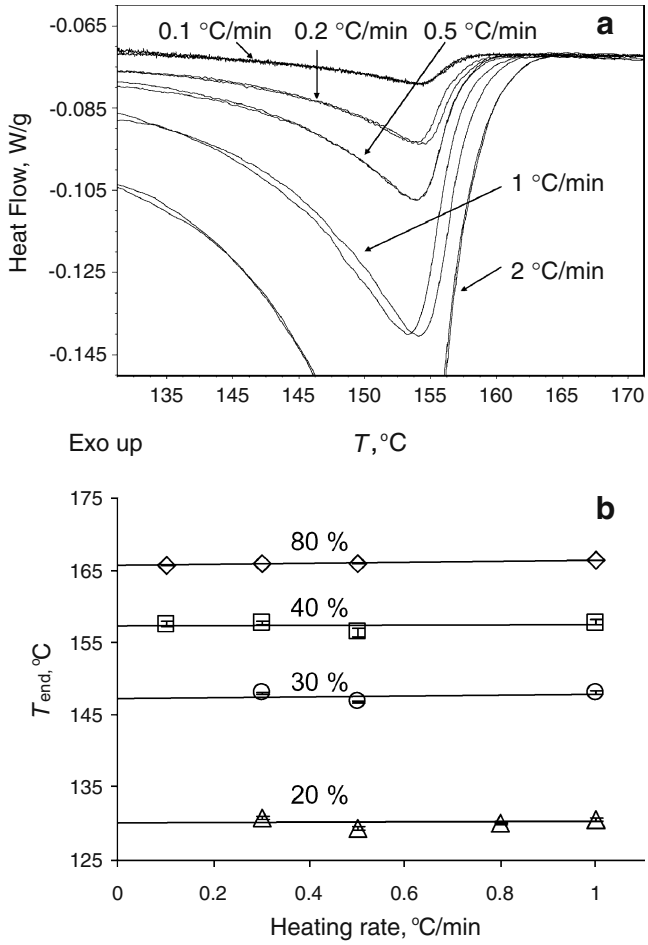

Fig. 2. **a** Dissolution endotherms measured at different heating rates for 40% *w/w* D-mannitol in PVP. **b** T_{end} extrapolation for D-mannitol in PVP K15 at different concentrations (80%, 40%, 30% and 20% *w/w*).

Cryomilling is known to make a crystalline material partially or fully amorphous (19); in this study, cryomilling rendered the solute partially amorphous before its dissolution endpoint was measured. A pertinent question therefore is how the amorphous solute affects the determination of the dissolution endpoint of the crystalline solute. If the amorphous solute was already dissolved in the polymer, it would not yield a dissolution endotherm. If the amorphous solute is not dissolved in the polymer, it may show a liquid–liquid mixing event that is less energetic and at a lower temperature than the dissolution endotherm of the crystalline solute. The presence of the amorphous solute is expected to reduce the intensity of the dissolution endotherm of the crystalline solute but not to alter the dissolution endpoint of the crystalline solute. We show later that in the case of IMC in PVP/VA, cryomilling for long times made the crystalline solute completely amorphous. The fully amorphous IMC/PVP/VA mixture showed no significant thermal events near T_{end} (see Fig. 10a later), indicating the presence of an amorphous solute would not affect the determination of the dissolution endpoint of the crystalline solute.

It is also pertinent to consider whether the particle size reduction caused by cryomilling alters the melting or dissolution temperature of crystals. To test this effect, we cryomilled pure D-mannitol crystals (β polymorph) for the same time as in preparing solute/polymer mixtures and analyzed the product by DSC. We observed no significant effect of cryomilling on the melting point of D-mannitol.

Solubility of D-Mannitol in PVP near T_g Measured by the DSC Dissolution-Endpoint Method

Having established cryomilling as a suitable method for sample preparation, we applied it to measure the solubility of D-mannitol in PVP. The typical raw data collected are shown in Fig. 2 and the T_{end} *vs.* concentration relation is shown in Fig. 3. The procedure could be carried out with reasonable confidence down to 20% *w/w* D-mannitol in PVP. At still lower concentrations, the procedure was difficult to carry out because the dissolution endotherm became too weak and the solution was too viscous for the dissolution endpoint to be determined with confidence.

The last point can be appreciated by comparing the T_{end}–composition curve and the T_g–composition curve (Fig. 3). T_g is the temperature at which a liquid loses its ability to flow (its viscosity reaches ca. 10^{12} Pa s) and can be readily measured by DSC. To determine the T_g–composition curve, we first heated a D-mannitol/PVP mixture of known composition to produce a homogeneous solution and then heated the solution a second time to measure its T_g. The T_g shown in Fig. 3 is the inflection point of the glass transition measured by DSC. The T_g–composition curve changes from T_g=10°C for pure D-mannitol (20) to $T_g \approx 110$°C for PVP. It is important to note that the T_g in Fig. 3 was *not* obtained in the same scan used to determine T_{end}; the T_g could be

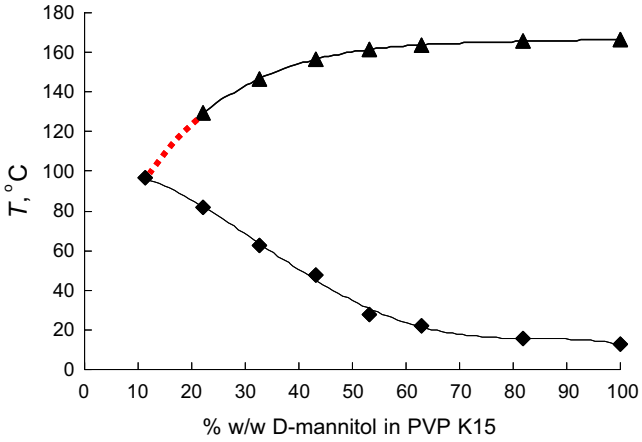

Fig. 3. The T_{end} (*triangle*) and T_g (*diamond*) as a function of D-mannitol concentration. The *dashed curve* extrapolates the observed data to the T_g curve. The crossing point gives the solubility for which the saturated solution is at T_g.

determined by scanning the sample a second time after the T_{end} measurement, but was actually determined with a separate series of samples and DSC runs.

The quantity (T_{end}–T_g) for a given composition defines how close the dissolution endpoint T_{end} is to the glass transition temperature T_g of the saturated solution (the solution in which the last trace of D-mannitol crystals dissolves). At a high D-mannitol concentration, (T_{end}–T_g) is large, the viscosity of the saturated solution is low, and the dissolution process is kinetically facile. For such mixtures, we observed that the T_{end} did not depend strongly on the heating rate (Fig. 2). As the D-mannitol concentration decreases, (T_{end}–T_g) decreases and the viscosity of the saturated solution increases. At low enough D-mannitol concentration, dissolution eventually becomes too slow for the system to achieve solubility equilibrium even at the slowest heating rate practical. For such systems, T_{end} changed rapidly and non-linearly with the heating rate, making the extrapolation to zero heating rate less confident. The inability to reach solubility equilibrium owing to slow liquid dynamics ultimately defines the limit of the DSC method. At the lowest D-mannitol concentration of our measurement (20% *w*/*w*), T_{end} is ca. 50°C above the T_g of the saturated solution. Despite this limitation, the method enabled us to get sufficiently close to T_g to estimate the solubility of D-mannitol in PVP near T_g by extrapolation. In this way we found that the solubility of crystalline D-mannitol (β polymorph) in PVP is 13% *w*/*w* at 105°C and 11% *w*/*w* at 97°C. According to this analysis, at 97°C, the saturated solution exists at the glass transition temperature.

Validation of the DSC Dissolution-Endpoint Method for the D-Mannitol/PVP System

To verify the solubility of D-mannitol in PVP obtained with the DSC method (hereafter referred to as Method I, Fig. 4), we used two other solubility-indicating methods, Methods II and III. In Method II, a solution of D-mannitol/PVP was prepared (by cryomilling and melting) at a concentration higher than the predicted solubility for some temperature. The solution was then aged to see whether crystallization occurred over time, thereby determining whether the solution was supersaturated. We tracked three indicators of crystallization: (a) the glass transition temperature T_g of the mixture, which is expected to increase when D-mannitol crystallizes from its mixture with PVP (Fig. 3); (b) the dissolution endotherm of D-mannitol crystals formed during aging; and (c) new crystals observable by polarized light microscopy. In Method III, D-mannitol was dissolved in PVP at high enough concentration so that D-mannitol rapidly crystallized (in seconds) soon after the molten mixture was cooled. This crystallization would seed the remaining amorphous phase with crystals for further crystallization during aging. Because Method III introduced crystal seeds at time zero, the time required to reach solubility equilibrium with Method III might be shorter than that with Method II, which required an induction time for nucleation (Fig. 4).

We chose 105°C as the temperature for these tests, at which the predicted solubility is 13% *w*/*w*. For Method II, D-mannitol was mixed with PVP by cryomilling at 30% *w*/*w*. The mixture was melted in several DSC pans on a microscope hot stage. The resulting solution was hermetically sealed and aged at 105°C. The mixture was analyzed by DSC at times ranging from a few days to 155 days. We observed that the T_g of the mixture increased upon aging (Fig. 5a). Simultaneously, an endotherm appeared near 155°C, which resulted from the dissolution of D-mannitol crystals formed during aging at 105°C. These crystals belonged to the δ polymorph; this was confirmed by their melting point (slightly lowered by the presence of the polymer) (Fig. 5a), by Raman microscopy, and by X-ray diffraction (Fig. 6). In 155 days, the T_g of the amorphous portion of the mixture increased from 70°C to approximately 95°C and the step size of the glass transition became smaller, indicating the amount of the amorphous phase became smaller. Meanwhile, the area of the dissolution endotherm

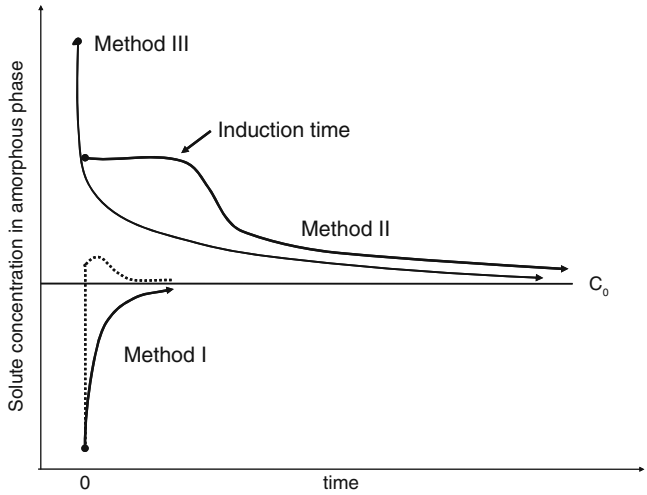

Fig. 4. Three methods to estimate the solubility of D-mannitol in PVP. Method I measures dissolution endpoint by DSC of mixture of concentration C_0. *Dotted line* indicates local overheating. Method II monitors the crystallization of a moderately supersaturated solution whose crystallization requires an induction time. In Method III, the crystallization of a highly supersaturated solution is quickly initiated (short induction time) and further crystallization is monitored with aging.

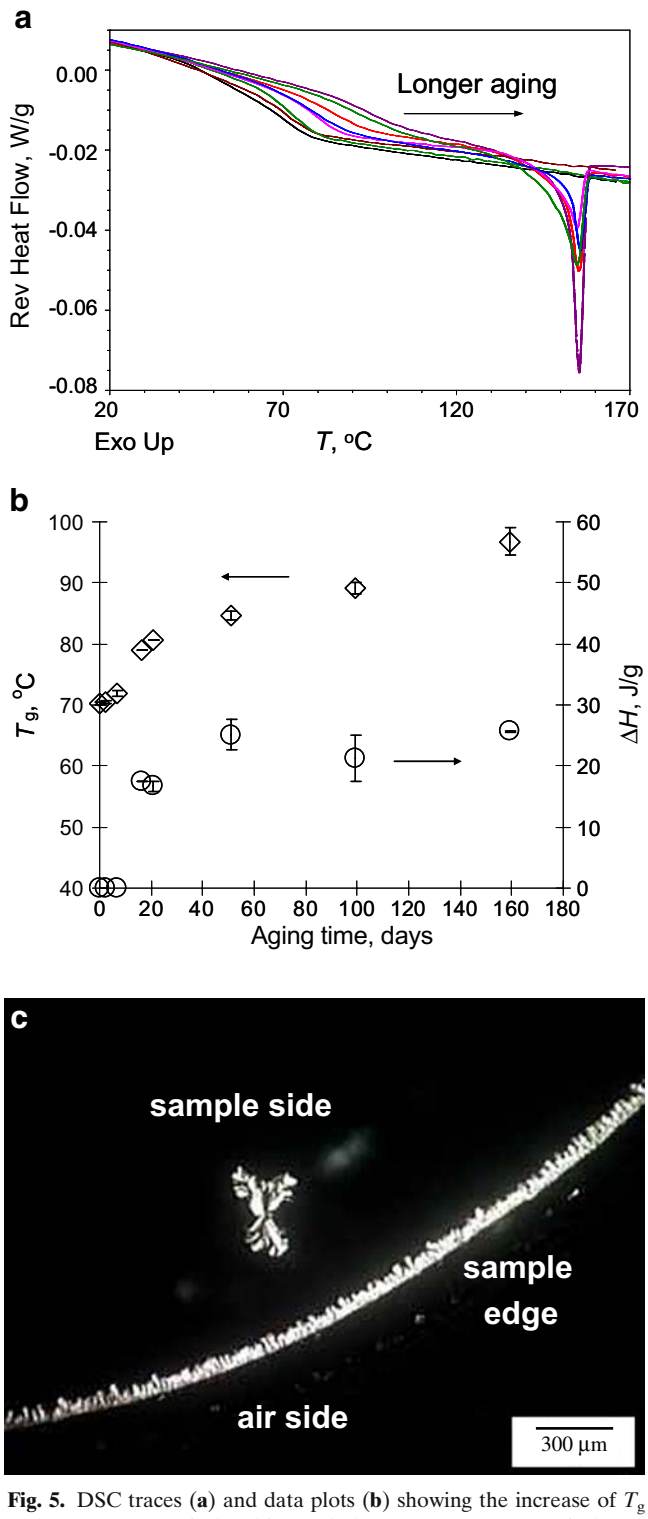

Fig. 5. DSC traces (**a**) and data plots (**b**) showing the increase of T_g and area of D-mannitol melting endotherm of a 30% D-mannitol/PVP mixture with aging time at 105°C. **c** D-mannitol crystals formed from the supersaturated solution during aging. They were viewed through a light microscope between crossed-polarizers.

of D-mannitol increased (Fig. 5b). Visual observation verified that the 30% *w/w* D-mannitol in PVP was initially free of crystals but on aging at 105°C yielded crystals of D-mannitol (Fig. 5c). Most crystals were observed at the sample/air interface, but some were observed in the interior of the liquid (Fig. 5c). These results confirm that the 30% *w/w* solution of D-mannitol in PVP is indeed supersaturated at 105°C. Moreover, the results show that after crystallizing a 30% *w/w* D-mannitol/PVP solution at 105°C for 155 days, the remaining amorphous phase contained approximately 12% *w/w* of D-mannitol (reading from the T_g–composition curve in Fig. 3 for T_g=95°C). If solubility equilibrium had been reached after this long aging, the D-mannitol concentration in the amorphous phase (12% *w/w*) would be its solubility at 105°C. This value approximately matches the solubility estimated with Method I (13% *w/w* at 105°C).

Note that in Method II, the solution concentration approached the solubility of δ D-mannitol during crystallization, not the solubility of β D-mannitol as measured in Method I. The solubilities of D-mannitol polymorphs, however, are similar because of their relatively small free-energy difference (21). For example, from $G_\delta - G_\beta \approx 1.0\,kJ/mol$ at 105°C (15) and the equation $G_\delta - G_\beta = RT \ln x_\delta/x_\beta$, the solubility of the δ polymorph is estimated to be 35% higher than that of the β polymorph at 105°C.

To carry out Method III, 60% *w/w* D-mannitol was first dissolved in PVP by cryomilling and melting. The liquid was cooled to 110°C and crystallized in seconds. Visual observation and melting-point determination by DSC confirmed that crystals of D-mannitol's δ polymorph formed throughout the material (22,23). This fast crystallization, though occurring everywhere, did not completely crystallize all the D-mannitol above the saturation limit and the remaining amorphous phase was still supersaturated. Different from the amorphous phase in Method II, this amorphous phase was in uniform contact with D-mannitol crystals formed throughout the liquid

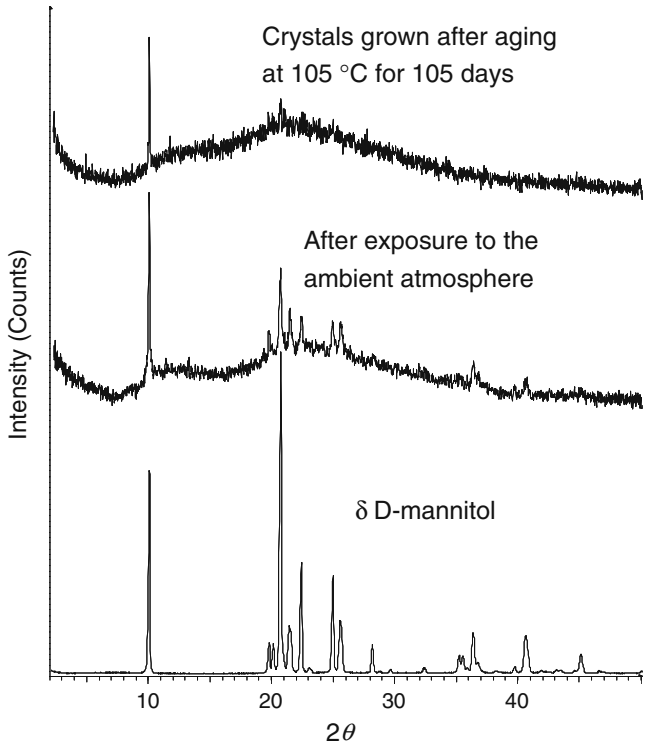

Fig. 6. XRD pattern of D-mannitol crystals formed in 30% *w/w* D-mannitol/PVP solution during aging at 105°C (*top*) compared with that of δ polymorph (*bottom*). More δ crystals grew in the sample after exposure to the ambient atmosphere (*middle*).

before the aging step began. Upon aging at 105°C, D-mannitol crystallized further, with pre-existing crystals serving as seeds. Fig. 7 shows that after 2 days of aging at 105°C, T_g increased by ca. 10°C. This rate of T_g increase was faster than that observed with Method II (Fig. 7). With longer aging, the T_g continued to rise and leveled off after approximately 50 days. Due to the lower polymer concentration and thus the smaller fraction of the amorphous phase, the glass transition was weaker and more difficult to measure in Method III than in Method II. With longer aging, the amount of the amorphous phase decreased further; after 50 days, it was difficult to determine the glass transition with confidence even though data were collected up to 155 days of aging. Within the errors of these experiments, the results of Methods II and III support the conclusion reached with Method I.

Further Test of the DSC Dissolution-Endpoint Method for the NIF/NMP System

Marsac *et al*. reported that the solubility of NIF in NMP is 17.4% *w*/*w* at 25°C (3). To further test the DSC dissolution-endpoint method (Method I), we applied it to the NIF/NMP system, a small-molecule solute/small-molecule solvent system. In the process of this work, we found that NIF forms a 1:1 solvate with NMP, which is less soluble in NMP than the anhydrous α NIF. Fig. 8 shows the TGA and XRD data of the NIF/NMP solvate. The reported NIF/NMP solubility is presumably that of the NIF/NMP solvate, not the anhydrous NIF. Fig. 9 shows the solubility of the NIF/NMP solvate in NMP measured with Method I and the literature value. We verified that at the relevant dissolution endpoints, the stable NIF crystalline phase is the NIF/NMP solvate; this was done by aging the NIF/NMP slurry at those temperatures and harvesting the resulting crystals for XRD. The data of NIF/NMP solubility measured by DSC agree well with the reported value (Fig. 9).

Solubility of IMC and NIF in PVP/VA Near the Glass Transition Temperatures

We next applied the DSC dissolution-endpoint method (Method I) to measure the solubility of NIF and IMC in PVP/VA. As in the case of D-mannitol/PVP, cryomilling was used

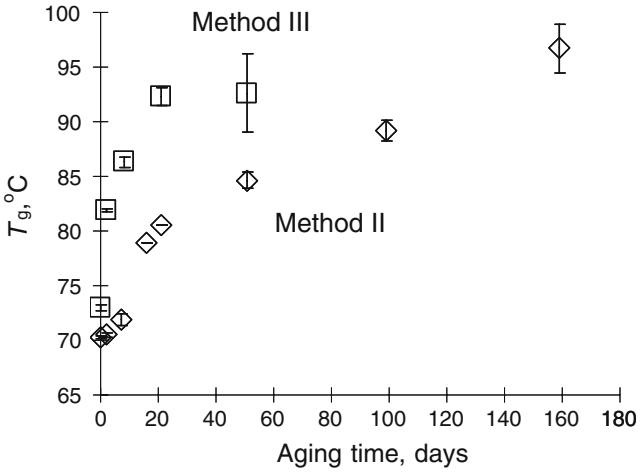

Fig. 7. Comparison of T_g increase observed with Methods II and III.

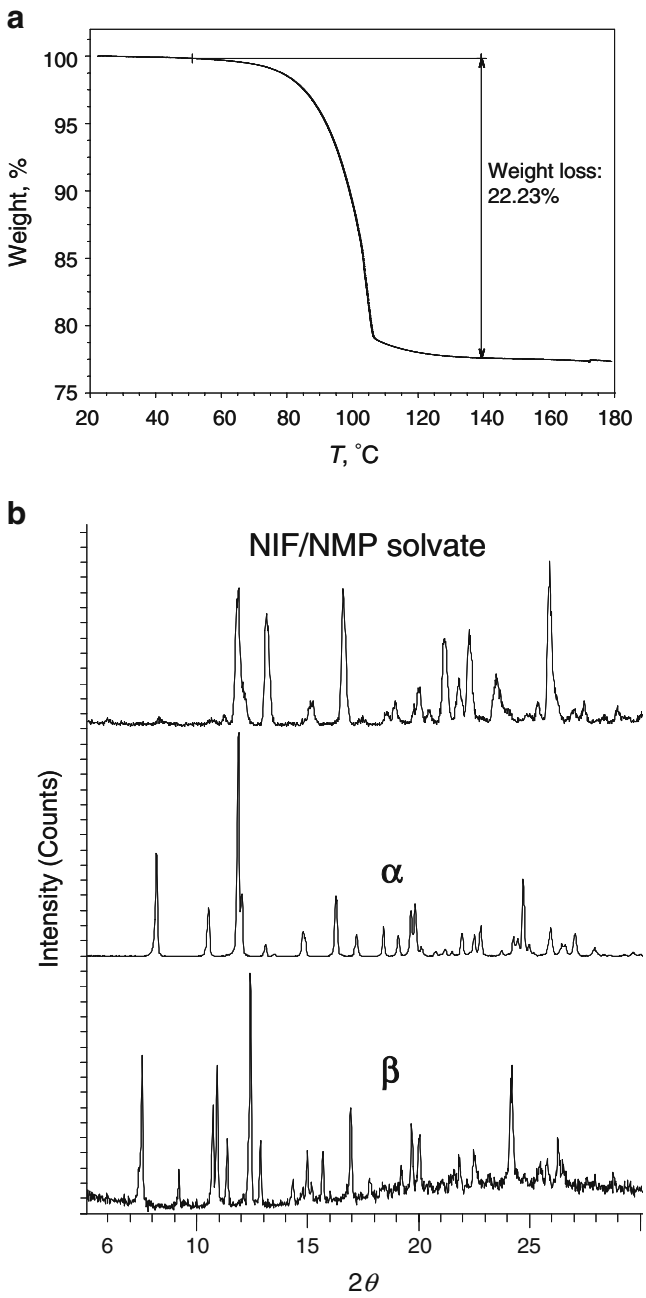

Fig. 8. **a** TGA of the NIF/NMP solvate showing 22.2% weight loss upon heating. The amount of NMP in a 1:1 solvate is 99.13/(99.13+346.34)=22.25%. **b** XRD pattern of the NIF/NMP solvate compared with those of the anhydrous polymorphs of NIF.

to prepare drug/polymer mixtures. The crystals of the γ polymorph of IMC and of the α polymorph of NIF were used to prepare drug/polymer mixtures. XRD analysis showed that the crystals that remained after cryomilling were of the original polymorphs. Because the polymorph used was the monotropically most stable for each system, no polymorphic conversion could occur during DSC analysis.

The cryomilling time was similarly optimized for these systems as for D-mannitol/PVP. As in the case of D-mannitol/PVP, cryomilling facilitated the determination of dissolution endpoints T_{end}. Fig. 10a illustrates this effect for the mixture

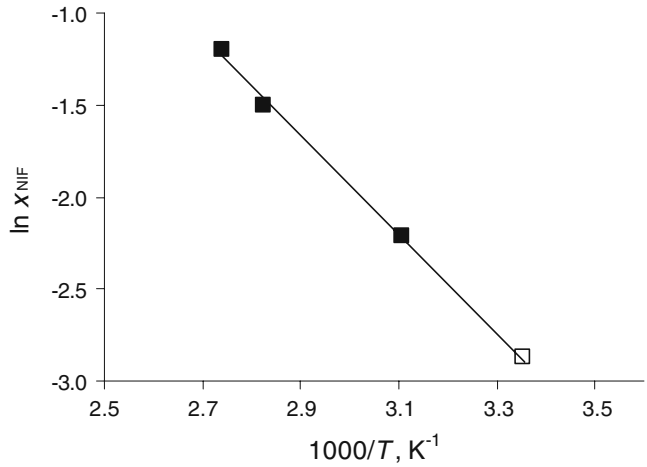

Fig. 9. Solubility of the NIF/NMP solvate in NMP measured by Method I (*solid symbol*) and the literature value at 25°C (*empty symbol*).

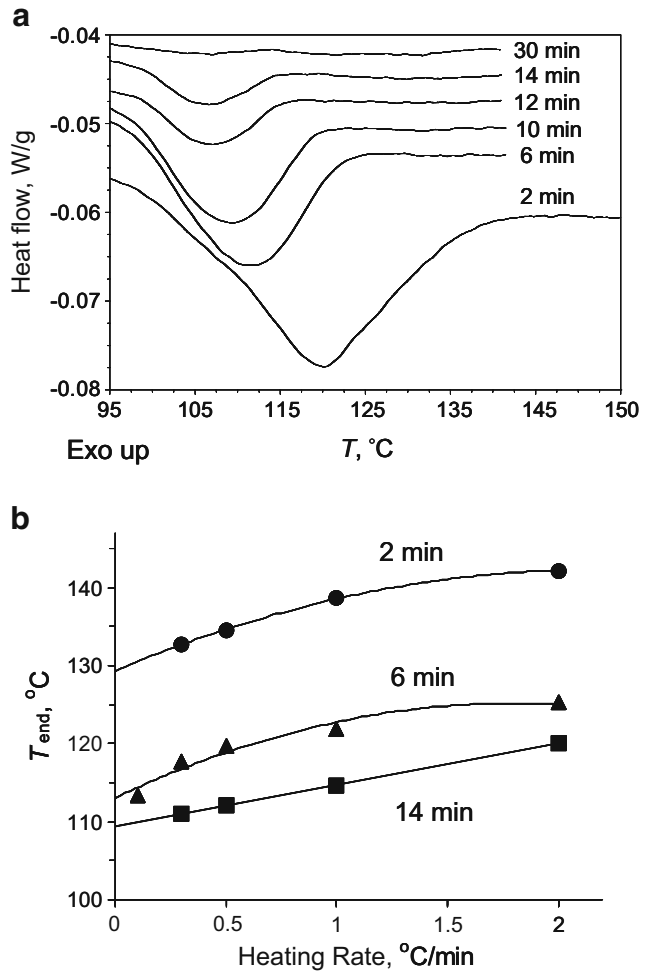

Fig. 10. a Dissolution endotherms for 40% *w/w* IMC in PVP/VA after cryomilling for different times (heating rate=1°C/min). **b** The dissolution endpoints of 40% *w/w* IMC in PVP/VA as a function of heating rates after cryomilling for different times.

of 40% *w/w* IMC in PVP/VA. Longer cryomilling led to lower T_{end} and smaller dissolution endotherm. The T_{end} decreased with the milling time up to approximately 12 min. Fig. 10b illustrates an additional effect of cryomilling: for the mixtures milled for shorter times (2 and 6 min), T_{end} changed non-linearly with DSC heating rate, whereas for a mixture milled sufficiently long (14 min), T_{end} changed more linearly with heating rate, making the extrapolation to zero heating rate more confident.

Unlike the D-mannitol/PVP system, the maximal milling times for these two systems were limited by how long the drug could be milled without completely losing crystallinity (cryomilling IMC alone can completely destroy its crystallinity (19)). For 40% *w/w* IMC in PVP/VA, 30 min milling was long enough to completely destroy the crystallinity of the solute. DSC analysis of this over-milled mixture found no significant thermal events near the dissolution temperature of the crystalline solute (Fig. 10a, top curve). This observation supports the point made earlier that the presence of an amorphous solute produced by milling does not significantly affect the determination of the dissolution endpoint of the crystalline solute. The final cryomilling time chosen was 14 min for 40% IMC in PVP/VA and 20 min for 25% NIF in PVP/VA.

Fig. 11 shows how the dissolution endpoint T_{end} and the glass transition temperature T_g (onset) changed with the drug concentration for the two systems. The lowest drug concentration for which T_{end} could be measured was 40% *w/w* IMC in PVP/VA and 25% *w/w* NIF in PVP/VA. The corresponding T_{end} was 33°C above T_g for the IMC-PVP/VA system and 34°C above T_g for the NIF-PVP/VA system. As in the case of D-mannitol/PVP, these lower concentration limits existed because of the increasing viscosity as the solution's T_g is approached, making it difficult to achieve solubility equilibrium during the DSC scan. Nonetheless, our measurements have approached the T_g sufficiently to allow an estimation by

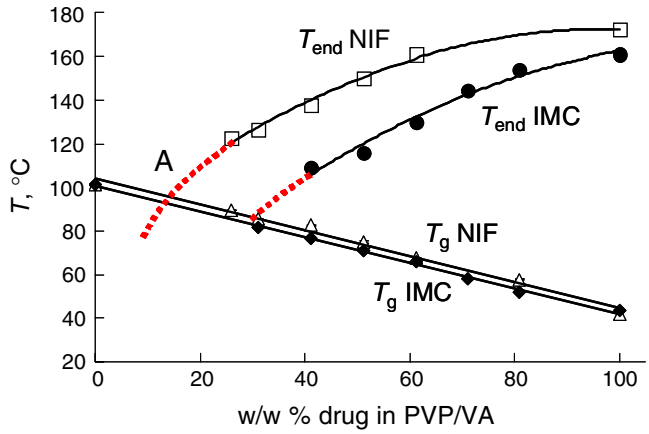

Fig. 11. Dissolution endpoints T_{end} and glass transition temperatures T_g of IMC/PVP/VA and NIF/PVP/VA *vs.* solute concentration. The T_{end} values refer to the γ polymorph of IMC and the α polymorph of NIF. For each system, the *dashed curve* extrapolates the observed data to lower temperatures. The intersection of the T_{end} and T_g curves gives the solubility for which the saturated solution is at T_g. Extending the T_{end} curve below the T_g curve (as shown for NIF) predicts the equilibrium solubility at temperatures at which saturated solute/polymer solutions are normally glasses. The intersecting T_{end} and T_g curves divide the *T*-composition space into four regions, which are discussed in text.

extrapolation (dashed curves in Fig. 11) of the solubilities of IMC and NIF in PVP/VA at temperatures at which the saturated solutions exist at T_g. We found that the solubility of IMC in PVP/VA is approximately 28% *w/w* at 85°C and this saturated solution exists at T_g. We found that the solubility of NIF in PVP/VA is approximately 12% *w/w* at 95°C and this saturated solution exists at T_g.

Fig. 12 compares the solubilities determined for the three systems of this study in the format of ln *x* (mole fraction) *vs.* $1/T$: D-mannitol in PVP, IMC in PVP/VA, and NIF in PVP/VA. At the same temperature, the molar solubility of IMC in PVP/VA is higher than NIF in PVP/VA and the molar solubility of D-mannitol in PVP is lower than those of IMC and NIF in PVP/VA. In all three systems, the observed solubility exceeds substantially the ideal solubility. It is unclear why the ln x–$1/T$ plot is more curved for D-mannitol in PVP than for the other two systems.

Significance of Solubility at T_g and the T_{end}/T_g Diagram

This study has determined the solubility of small-molecule crystals in polymers near T_g and by extrapolation, obtained the solubility at T_g, a quantity defined as the solubility at the temperature at which the crystalline phase is in equilibrium with a saturated solution that exists at its T_g. The solubility at T_g is 11% *w/w* for D-mannitol in PVP with T_g=97°C (Fig. 3), 28% *w/w* for indomethacin in PVP/VA with T_g=85°C (Fig. 11), and 12% *w/w* for nifedipine in PVP/VA with T_g=95°C (Fig. 11). It would be desirable to determine the solubility at even lower temperatures (e.g., room temperature), at which the saturated solution is an amorphous solid (glass). Such a task will need to confront the problem of slow molecular diffusion. To appreciate this problem, recall that the self-diffusion coefficient of a small-molecule liquid at T_g is on the order of 10^{-16} cm^2/s (24). The time required for molecules to diffuse 100 nm on average is $(10^{-5}\text{ cm})^2/(2\times10^{-16}\text{ cm}^2/\text{s})$=6 days. The process of dissolution below T_g may be too slow to be measured by scanning calorimetry and other approaches may be needed.

Extending the T_{end} curve below the T_g curve (as shown in Fig. 11 for NIF/PVP/VA) yields a prediction of the equilibrium solubility at temperatures at which saturated solute/polymer solutions are normally glasses. It is important to emphasize that the solubility thus obtained is an *equilibrium* solubility, for which the saturated solution is an equilibrium liquid, not a kinetically frozen glass. Glasses are the usual physical form of amorphous formulations; a glass relaxes toward the equilibrium liquid over time. Because a glass changes over time but solubility is an equilibrium property, solubility in a glassy matrix is poorly defined. It is reasonable to define an apparent solubility if glass relaxation is slow. This apparent solubility is higher than the equilibrium solubility and decreases as the glass matrix relaxes; when it relaxes all the way to the equilibrium liquid state, the appropriate solubility is the equilibrium solubility (obtained by extending the T_{end} curve below the T_g curve). This solubility is the thermodynamically safe drug loading below which there is no risk of crystallization. But attaining equilibrium in the glassy state might be so slow that it could be unnecessarily conservative to insist on drug loadings that are below equilibrium solubilities.

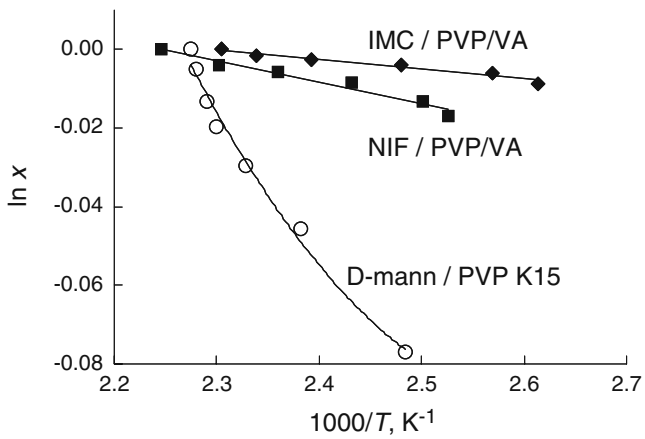

Fig. 12. Solubility–temperature relations for the three systems studied. The fitting curves are guide to the eye.

The T_{end}/T_g diagram (Figs. 3 and 11) indicates whether a solute/polymer solution is able or unable to crystallize and whether it is a liquid or a glass. If the T_{end} curve is extended to below the T_g curve, each of the three systems studied features two intersecting T_{end} and T_g curves, which defines four temperature–composition regions. We label these four regions A, B, C, and D, starting from the region above the T_{end} and T_g curves and moving clockwise (A is shown in Fig. 11 for NIF in PVP/VA). Region A is characterized by $T>T_{end}$ and $T>T_g$; in this region, the solute/polymer solution is a liquid and unable to crystallize. Region B is characterized by $T_g<T<T_{end}$; in this region, the solute/polymer solution is a liquid and able to crystallize. Region C is characterized by $T<T_{end}$ and $T<T_g$; in this region, the solute/polymer solution is a glass and able to crystallize. Region D is characterized by $T_{end}<T<T_g$; in this region, the solute/polymer solution is a glass and unable to crystallize. To understand the "safety margin" of drug loading in polymer dispersions, it may be useful to assess the stability against crystallization using the T_{end}/T_g diagram as a reference. It could be especially interesting to study the stability of drug/polymer solutions in Region C, wherein the solute is supersaturated only in the low-mobility glassy state.

CONCLUSIONS

We have developed a DSC method for measuring the solubility of small-molecule crystals in polymeric matrices. The method relies on the detection of the dissolution endpoint of a drug/polymer mixture. Proper mixing of the drug and polymer components was found important for determining the equilibrium endpoints of dissolution. To this end, cryogenic milling proved an effective method for mixing components prior to DSC analysis. The DSC dissolution-endpoint method was validated against two independent, solubility-indicating methods for the D-mannitol/PVP system and against the literature solubility of NIF in NMP (a small-molecule solvent). We have applied the method to obtain for the first time the solubilities of several small-molecule crystals in polymers near the glass transition temperature T_g, including D-mannitol in PVP, indomethacin in PVP/VA, and nifedipine in PVP/VA. The lowest temperature at which the solubility could be evaluated with some confidence was approximately 30°C above T_g; at

even lower temperatures, the system was too viscous to achieve dissolution equilibrium in the timescale of DSC measurement. By extrapolation, the data allowed estimation of the solubility of small-molecule crystals in polymeric matrices at T_g. This method and its improved versions have the potential of providing useful data for designing physically stable formulations of amorphous drugs.

ACKNOWLEDGMENT

We thank Abbott Laboratories for supporting this work and Dr. Feng Qian of BMS for the helpful discussions about the T_{end}/T_g diagrams.

REFERENCES

1. M. Vasanthavada, W. Tong, Y. Joshi, and M. S. Kislalioglu. Phase behavior of amorphous molecular dispersions I: determination of the degree and mechanism of solid solubility. *Pharm. Res*. **21**:1598–1606 (2004).
2. M. Vasanthavada, W. Tong, Y. Joshi, and M. S. Kislalioglu. Phase behavior of amorphous molecular dispersions II: role of hydrogen bonding in solid solubility and phase separation kinetics. *Pharm. Res*. **22**:440–448 (2004).
3. P. J. Marsac, S. L. Shamblin, and L. S. Taylor. Theoretical and practical approaches for prediction of drug–polymer miscibility and solubility. *Pharm. Res*. **23**:2417–2426 (2006).
4. P. J. Marsac, T. Li, and L. S. Taylor. Estimation of drug–polymer miscibility and solubility in amorphous solid dispersions using experimentally determined interaction parameters. *Pharm. Res*. in press (2008).
5. R. Mohan, H. Lorenz, and A. S. Myerson. Solubility measurement using differential scanning calorimetry. *Ind. Eng. Chem. Res*. **41**:4854–4862 (2002).
6. K. Park, J. M. B. Evans, and A. S. Myerson. Determination of solubility of polymorphs using differential scanning calorimetry. *Cryst. Growth Des*. **3**:991–995 (2003).
7. R. Tamagawa, W. Martins, S. Derenzo, A. Bernardo, M. Rolemberg, P. Carvan, and M. Giulietti. Short-cut method to predict the solubility of organic molecules in aqueous and nonaqueous solutions by differential scanning calorimetry. *Cryst. Growth Des*. **6**:313–320 (2006).
8. V. Andronis, and G. Zografi. Crystal nucleation and growth of indomethacin polymorphs from the amorphous state. *J. Non-Cryst. Solids*. **271**:236–248 (2000).
9. V. Andronis, and G. Zografi. Molecular mobility of supercooled amorphous indomethacin, determined by dynamic mechanical analysis. *Pharm. Res*. **14**:410–419 (1997).
10. M. Yoshioka, B. C. Hancock, and G. Zografi. Crystallization of indomethacin from the amorphous state below and above its glass transition temperature. *J. Pharm. Sci*. **83**:1700–1705 (1994).
11. T. Wu, and L. Yu. Origin of enhanced crystal growth kinetics near Tg probed with indomethacin polymorphs. *J. Phys. Chem. B*. **110**:15694–15699 (2006).
12. S. R. Vippagunta, K. A. Maul, S. Tallavajhala, and D. J. W. Grant. Solid-state characterization of nifedipine solid dispersions. *Int. J. Pharm*. **236**:111–123 (2002).
13. N. Zajc, A. Obreza, M. Bele, and S. Srcic. Physical properties and dissolution behaviour of nifedipine/mannitol solid dispersions prepared by hot melt method. *Int. J. Pharm*. **291**:51–58 (2005).
14. I. Sugimoto, A. Kuchiki, and H. Nakagawa. Stability of nifedipine–polyvinylpyrrolidone coprecipitate. *Chem. Pharm. Bull*. **29**:1715–1723 (1981).
15. H. Ishida, T. Wu, and L. Yu. Sudden rise of crystal growth rate of nifedipine near Tg without and with polyvinylpyrrolidone. *J. Pharm. Sci*. **96**:1131–1138 (2007).
16. L. S. Taylor, and G. Zografi. Spectroscopic characterization of interactions between PVP and indomethacin in amorphous molecular dispersions. *Pharm. Res*. **14**:1691–1698 (1997).
17. T. Matsumoto, and G. Zografi. Physical properties of solid molecular dispersions of indomethacin with poly(vinylpyrrolidone) and poly(vinylpyrrolidone-co-vinyl-acetate) in relation to indomethacin crystallization. *Pharm. Res*. **16**:1722–1728 (1999).
18. T. Miyazaki, S. Yoshioka, Y. Aso, and S. Kojima. Ability of polyvinylpyrrolidone and polyacrylic acid to inhibit the crystallization of amorphous acetaminophen. *J. Pharm. Sci*. **93**:2710–2717 (2004).
19. K. J. Crowley, and G. Zografi. Cryogenic grinding of indomethacin polymorphs and solvates: assessment of amorphous phase formation and amorphous phase physical stability. *J. Pharm. Sci*. **91**:492–507 (2002).
20. L. Yu, D. S. Mishra, and D. R. Rigsbee. Determination of the glass properties of D-mannitol using sorbitol as an impurity. *J. Pharm. Sci*. **87**:774–777 (1998).
21. L. Yu, J. Huang, and K. J. Jones. Measuring free-energy difference between crystal polymorphs through eutectic melting. *J. Phys. Chem. B*. **109**:19915–19922 (2005).
22. L. Yu. Nucleation of one polymorph by another. *J. Am. Chem. Soc*. **125**:6380–6381 (2003).
23. J. Tao, and L. Yu. Kinetics of cross-nucleation between polymorphs. *J. Phys. Chem. B*. **110**:7097–7101 (2006).
24. M. K. Mapes, S. F. Swallen, and M. D. Ediger. Self-diffusion of supercooled *o*-terphenyl near the glass transition temperature. *J. Phys. Chem. B*. **110**:507–511 (2006).